

# Locally Adaptive Random Walk Stochastic Volatility

Jason B. Cho\*

Department of Statistics and Data Science, Cornell University  
and

David S. Matteson

Department of Statistics and Data Science, Cornell University

October 15, 2024

## Abstract

We introduce a novel Bayesian framework for estimating time-varying volatility by extending the Random Walk Stochastic Volatility (RWSV) model with a new Dynamic Shrinkage Process (DSP) in (log) variances. Unlike classical Stochastic Volatility or GARCH-type models with restrictive parametric stationarity assumptions, our proposed Adaptive Stochastic Volatility (ASV) model provides smooth yet dynamically adaptive estimates of evolving volatility and its uncertainty (vol of vol). We derive the theoretical properties of the proposed global-local shrinkage prior. Through simulation studies, we demonstrate that ASV exhibits remarkable misspecification resilience with low prediction error across various data generating scenarios in simulation. Furthermore, ASV's capacity to yield locally smooth and interpretable estimates facilitates a clearer understanding of underlying patterns and trends in volatility. Additionally, we propose and illustrate an extension for Bayesian Trend Filtering simultaneously in both mean and variance. Finally, we show that this attribute makes ASV a robust tool applicable across a wide range of disciplines, including in finance, environmental science, epidemiology, and medicine, among others.

*Keywords:* Time series; Trend filtering; Dynamic linear model;

---

\*The authors gratefully acknowledge financial support from *National Science Foundation grants OAC-1940124 and DMS-2114143*

# 1 Introduction

Volatility in a time series indicates how much the series deviates from its average value. Estimating volatility holds significant importance across diverse fields as it offers crucial insights into the underlying data generation process. In finance, for instance, understanding the volatility of financial assets is pivotal for derivative pricing, asset valuation, portfolio management, and overall risk assessment. In epidemiology, estimating the volatility of new disease cases enables early detection of major outbreaks (Kostoulas et al. [2021]) and enhances predictions of number of new cases (Achcar et al. [2020], Sarkar and Chatterjee [2017]). Climate scientists utilize time-varying volatility models to analyze various climate phenomena like tornadoes (Tippett [2014]), droughts (Modarres and Ouarda [2014]), and rainfall patterns (Mehdizadeh et al. [2017]). Similarly, in mechanical systems, volatility estimates derived from acceleration envelope readings aid in predicting machine failures (Pham and Yang [2010], Ma et al. [2017]). Additionally, in hydrology, understanding the volatility of river streamflows, which can vary drastically due to climate change, is achieved through time-varying volatility models (Wang et al. [2005, 2023a,b], Otache [2012]).

Commonly studied statistical models for estimating time-varying volatility include the Autoregressive Conditional Heteroskedasticity (ARCH) model [Engle, 1982], the Generalized ARCH (GARCH) model [Bollerslev, 1986], and the Stochastic Volatility (SV) model [Hull and White, 1987, Taylor, 2008, Melino and Turnbull, 1990]. However, these models, due to their parametric stationarity assumptions, often suffer from model misspecification, leading to inaccurate estimation, especially when the underlying volatility process undergoes gradual or abrupt changes. Unfortunately, such changes are commonplace across various disciplines, rendering volatility estimates from these models unreliable. In finance, empirical studies by Chou [1988], French et al. [1987], Poon and Taylor [1992], So et al.

[1997], Su and Wang [2020] and Nishino and Kakamu [2015] all point to changes in underlying volatility process evidenced by high persistence. Similarly, scientists observe changes in volatility processes during extreme weather events (Tippett [2014]) attributed to climate change. In epidemiology, volatility in the number of new disease cases is expected to change due to seasonal effects or large outbreaks (Kostoulas et al. [2021]). Thus, there is a clear need for a flexible framework capable of adaptively estimating volatility, accommodating both gradual and abrupt changes.

A widely adopted strategy for accommodating changes in the underlying volatility process involves incorporating time-varying parameters into the aforementioned parametric models, thereby enhancing model flexibility. One of the popular methods to model time variation in parameters is via latent Markov switching models [Brunetti et al., 2008, Ardia et al., 2018, Caporale and Zekokh, 2019, Sajjad et al., 2008, Dueker, 1997]. Under this framework, parameters are time-varying and are assumed to originate from a fixed number of latent regimes, with transitions between regimes governed by a hidden Markov process. The inclusion of multiple regimes allows for greater flexibility compared to single-regime models. However, determining the number of latent regimes *a priori* remains a challenge. Additionally, estimating the latent regime at each time point as well as the transition probabilities between regimes adds to the complexity of parameter estimation. Note that the number of transition probabilities to be estimated grow quadratically with the number of regimes. Latent regime switching framework has been integrated into aforementioned parametric models such as the Markov-Switching ARCH by Hamilton and Susmel [1994] and Cai [1994], the Markov-Switching GARCH model by Bauwens et al. [2010] and Gray [1996], and the Markov-Switching SV model by So et al. [1998] and Hwang et al. [2004].

Herein, we present the Adaptive Stochastic Volatility (ASV) model, building upon the

Random Walk Stochastic Volatility (RWSV) model explored in Ruiz [1994] and Harvey et al. [1994]. RWSV commonly assumes the log-variance of the observed process follows a Gaussian random walk with a constant variance. In contrast, ASV introduces two significant modifications to RWSV: it incorporates a time-varying variance for the log-variance increments and adopts a global-local shrinkage prior for adaptability.

ASV’s local adaptability is a standout feature, effectively estimating volatility in the presence of gradual or abrupt changes in the volatility process with notable smoothness in between. It allows robustness against model misspecification, resulting in low prediction errors across diverse data-generating scenarios. In addition, ASV’s volatility estimates exhibit smoother trajectories compared to those generated by alternative time-varying parameter models. The reduction in noise within our estimates provides users with clearer insights into underlying patterns and trends in the data. We also propose an intermediary model, RWSV with a time-varying shrinkage prior but without the global-local structure, called RWSV with Bayesian LASSO (RWSV-BL). However, our results suggest that this model undersmooths and performs similarly to RWSV in most cases.

We specifically highlight a class of global-local shrinkage prior called Dynamic Shrinkage Processes (DSP) [Kowal et al., 2019], which includes dynamic versions of a horseshoe prior [Carvalho et al., 2010] as a special case. DSP has shown versatility across various applications. For example, Wu et al. [2024a] integrates DSP into a Bayesian dynamic linear model to estimate change points and score outliers. Another application is seen in Schafer and Matteson [2024], where DSP is used to propose the negative binomial Bayesian trend filter (NB-BTF) for adaptively smoothing integer-valued time series. Additionally, Wu et al. [2024b] combines the Bayesian trend filter with DSP and machine learning-based regularization method to effectively distinguish micro-level drifts from macro-level shifts.

Kowal et al. [2019] has also shown superior performance for trend filtering when compared against other shrinkage priors. DSP has been applied in the context of Stochastic Volatility in Mean (SVM) modeling [Huber and Pfarrhofer, 2021], where DSP is imposed on its time-varying regression on variance within the conditional mean of the process.

Section 2 introduces the model and its associated parameters; theoretical properties of DSP in comparison to other shrinkage priors are explored. Section 3 provides an overview of the Gibbs sampling scheme; Full conditional distributions are detailed in the supplementary material. Comparisons between proposed models on simulated data are presented in Section 4. Subsequently, Section 5 presents empirical analyses of three datasets: weekly log-returns on the S&P 500 index, weekly log-returns on EURO/USD exchange rate and weekly changes in death tolls from COVID-19 in the U.S. based on the proposed method. In Section 6, We propose Bayesian Trend Filter with Adaptive Stochastic Volatility (BTF-ASV) combining Bayesian Trend Filter with Dynamic Horseshoe Process (BTF-DHP) by Kowal et al. [2019] and Adaptive Stochastic Volatility model (ASV) proposed in this paper for simultaneously estimating both the time-varying means and the variances. The model is then applied to the surface air temperature anomaly data for empirical analysis.

## 2 Methodology

### 2.1 The Random Walk Stochastic Volatility Model

Our method, Adaptive Stochastic Volatility (ASV), may be thought of as an extension of Random Walk Stochastic Volatility (RWSV) model explored in Ruiz [1994] and Harvey et al. [1994]. Consider a zero mean process with  $T$  observations,  $\{y_t\}_{t=1}^T$ , and its log-variance term  $\{h_t\}_{t=1}^T$ . Stochastic Volatility (SV) model assumes the observed process  $y_t$  to follow a normal distribution with its log-variance term,  $h_t$ , following the lag order 1 autoregression. RWSV is a special case of SV model where the autoregressive coefficient is assumed to be

1. Thus, the model is defined as:

$$y_t = \exp\{h_t/2\}\epsilon_t \quad \epsilon_t \stackrel{iid}{\sim} N(0, 1)$$

$$\Delta h_t := h_t - h_{t-1} = \sigma_h u_t \quad u_t \stackrel{iid}{\sim} N(0, 1).$$

Unlike the SV model, RWSV is a unit-root non-stationary process. This assumption is substantiated by financial asset return analyses, as evidenced by several studies, including Chou [1988], French et al. [1987], Poon and Taylor [1992], So et al. [1997], Su and Wang [2020] and Nishino and Kakamu [2015], which consistently find that the autoregressive coefficient of the SV model fitted to stock market returns is close to 1. In RWSV,  $h_t$  is governed by a time-invariant variance term,  $\sigma_h^2$ , which determines the degree of variation between successive log-variances. A large  $\sigma_h^2$  implies high probability of significant changes in the  $h_t$  process, whereas a small  $\sigma_h^2$  indicates high probability of minimal to no changes in  $h_t$ . In a frequentist framework,  $\sigma_h$  is typically treated as a fixed parameter, often estimated via Quasi-Maximum Likelihood, as demonstrated in the original papers by Ruiz [1994] and Harvey et al. [1994]. More recent studies, such as that by Nishino and Kakamu [2015], have employed a Bayesian framework for estimation with a non-informative prior on  $\sigma_h^2$ .

## 2.2 Stochastic Volatility with Only Local Shrinkage

RWSV model, however, may provide a poor fit for time series exhibiting periods of both significant and minimal changes due to its assumption of a time-invariant  $\sigma_h^2$ . Ideally, we prefer  $\sigma_h^2$  to be time-varying, remaining small during periods of little to no significant changes and increasing to a large value during periods of abrupt changes in  $h_t$ . This problem is akin to high-dimensional regression problem as such model would require the number of parameters to be larger than the number of samples. A common frequentist approach to addressing this problem is by imposing an additional penalty term like the  $l_1$  penalty (Tibshirani [1996]). Similarly in Bayesian setting, sparsity inducing priors may be

imposed on the parameters. Drawing from Bayesian representations of LASSO as discussed in Park and Casella [2008] and the scale-mixture Gaussian representation of the Laplace distribution in West [1987], we propose an intermediary model called RWSV with Bayesian LASSO (RWSV-BL), which incorporates a time-varying variance for  $h_t$  as

$$\Delta h_t \sim N(0, \sigma_{h,t}^2) \quad \sigma_{h,t}^2 \stackrel{iid}{\sim} \text{Exp}\{(2\Lambda^2)^{-1}\}.$$

Under this Bayesian representation,  $\Delta h_t$  follows a normal distribution with one time-varying local parameter  $\sigma_{h,t}^2$ . RWSV-BL shares similarities with the  $l1$ -trend filter proposed by Kim et al. [2009] and Tibshirani [2014], which aims to provide a smooth estimate of the observed process  $y_t$ . The key distinction between the  $l1$ -trend filter and RWSV-BL lies in their respective focuses: while the  $l1$ -trend filter targets the estimation of the time-varying mean of the process, RWSV-BL is designed to estimate the time-varying log-variance,  $h_t$  instead. Drawing an analogy between the trend-filter and RWSV-BL allows us to conceptualize our problem as a smoothing task applied to the variance process. By incorporating shrinkage priors on the higher-order differences of the log-variance process, the model can achieve greater smoothing on  $h_t$ .

### 2.3 Adaptive Stochastic Volatility via Global-Local Shrinkage

Building upon the model in the previous subsection, we propose the Adaptive Stochastic Volatility (ASV) model. Unlike RWSV-BL, which consists of a time-varying local parameter, ASV features a global-local structure for the variance of the log-variance,  $\sigma_{h,t}^2$ . Specifically,  $\sigma_{h,t}$  is defined as  $\sigma_{h,t} := \tau \lambda_t$ , where  $\tau$  represents the global parameter, and  $\lambda_t$  represents the local parameter. The global parameter  $\tau$  controls the overall shrinkage and acts as the average shrinkage applied across all time points, while the local parameter  $\lambda_t$  controls smoothness at each time  $t$  in addition to  $\tau$ . The inclusion of the global parameter  $\tau$  enhances model smoothness by providing a consistent level of shrinkage across all

time points, which we find as essential in the application and simulations sections below. In contrast, the Bayesian LASSO model, as discussed in section 2.2 only incorporates a local parameter for  $\sigma_{h,t}^2$ . Section 5 shows ASV to yield significantly smoother estimates of  $h_t$  compared to RWSV-BL. Therefore, we propose the following model for estimating time-varying volatility:

$$\Delta^k h_t \sim N(0, \tau^2 \lambda_t^2) \quad \tau \sim \pi(\tau), \quad \lambda_t \stackrel{iid}{\sim} \pi(\lambda_t),$$

where  $k$  is usually set to 1 or 2, and  $\pi(\tau)$  and  $\pi(\lambda_t)$  represent priors on  $\tau$  and  $\lambda_t$ . Global-local shrinkage priors for Gaussian observations have been extensively studied in the past decade, particularly in the context of high-dimensional regression. Examples of such priors include the Horseshoe prior by Carvalho et al. [2010], the Horseshoe plus prior by Bhadra et al. [2015], the triple gamma prior by Cadonna et al. [2019], and Dynamic Shrinkage Processes (DSP) introduced by Kowal et al. [2019]. The global parameter,  $\tau$ , ensures that the estimate of  $h_t$  remains smooth overall, while the local parameter,  $\lambda_t$ , allows for local adaptivity in the presence of abrupt changes. Among the various aforementioned global-local priors, DSP are further analyzed and incorporated into the ASV model in this work. Two versions of ASV are explored: Adaptive Stochastic Volatility with Dynamic Horseshoe Prior (ASV-DHS) and Adaptive Stochastic Volatility with Horseshoe Prior (ASV-HP), the latter of which can be considered a special case of ASV-DHS.

## 2.4 Properties of Dynamic Shrinkage Processes

DSP distinguish themselves among global-local priors by incorporating temporal dependence in the local shrinkage parameter  $\lambda_t$ , allowing for a dynamic shrinkage approach. Kowal et al. [2019] applied DSP in Bayesian trend filtering and demonstrated its superior performance in terms of prediction error when estimating the mean of an arbitrary time series, compared to other well-studied horseshoe prior. Therefore, we focus on DSP as the



prior distribution on  $h_t$ . Under this framework,  $h_t \sim N(0, \sigma_{h,t}^2)$  and the priors on  $\sigma_{h,t}$  are defined by its log-squared term,  $v_t := \log(\sigma_{h,t}^2)$ :

$$v_t = \mu + \psi_t + \eta_t \quad \eta_t \stackrel{iid}{\sim} Z(a, b, 0, 1),$$

where  $Z$ -distribution has the following density function (Barndorff-Nielsen et al. [1982]):

$$f(z|a, b, \mu_z, \sigma_z) = (\sigma_z \beta(a, b))^{-1} \left( \exp\left\{ \frac{z - \mu_z}{\sigma_z} \right\} \right)^a \left( 1 + \exp\left\{ \frac{z - \mu_z}{\sigma_z} \right\} \right)^{-(a+b)}.$$

For the global parameter,  $\tau = \exp\{\mu/2\}$  and  $\lambda_t = \exp\{(\psi_t + \eta_t)/2\}$  represents the local parameter. Specifically,  $\psi_t$  models the temporal dependence of the process. A few candidate models for  $\psi_t$  includes the Hidden Markov Models, linear regression, or spline. For simplicity, the serial dependence is assumed to be positive, indicating that large  $\sigma_{h,t}^2$  is likely to result in large  $\sigma_{h,t+1}^2$ . Heuristic interpretation of this assumption is that large changes is likely to be followed by another large changes, while small changes is likely to be followed by small changes. Thus,  $\psi_t := \phi(v_t - \mu)$ , with  $\eta_t \sim Z(a, b, 0, 1)$  corresponding to the i.i.d scale parameter. The benefit of having  $Z$ -distribution as prior on  $\eta_t$  is its shrinkage property. By setting  $a = b = 1/2$  and  $\phi = 0$ , we have the horseshoe prior (Carvalho et al. [2010]), as  $\lambda_t = \exp\{\eta_t/2\} \sim C^+(0, 1)$  is equivalent to  $\eta_t \sim Z(1/2, 1/2, 0, 1)$ .

Owing to its autoregressive structure, the shrinkage profile of DSP is analyzed conditional on either the previous shrinkage term  $\kappa_t := \frac{1}{1 + \exp\{v_t\}}$  or the local scale parameter  $\lambda_t$ , which both follow Three Parameter Beta distribution (Kowal et al. [2019]). We consider the shrinkage profile of the stationary distribution of  $v_t$ . We show that DSP has similar properties as Horseshoe prior but induces heavier shrinkage. Let's first define  $z_{t,h} := \phi^h \eta_{t-h}$ .

Infinite order Moving Average representation of  $v_t$  results in:

$$\begin{aligned}
v_t &= \mu + \phi(v_{t-1} - \mu) + \eta_t & \eta_t &\sim Z(1/2, 1/2, 0, 1) \\
&= \mu + \sum_{h=0}^{\infty} \phi^h \eta_{t-h} \\
&= \mu + \sum_{h=0}^{\infty} z_{t,h}.
\end{aligned}$$

As shown in Barndorff-Nielsen et al. [1982],  $z_{t,h}$  is a scaled Hyperbolic Secant Distribution, with  $E(z_{t,h}|\phi) = 0$  and  $Var(z_{t,h}|\phi) = (|\phi|^h \pi)^2$ . Let's consider  $z_t := \sum_{h=0}^{\infty} z_{t,h}$ .

**Theorem 1.**  $z_t$  converges almost surely if and only if  $|\phi| < 1$ .

*Proof.* This directly follows from Kolmogorov's three series theorem. Note that the variance  $\sum_{h=0}^{\infty} var(z_{t,h}|\phi)$  converges if and only if  $|\phi| < 1$ . Exact derivation is explored in Appendix A.1. □

**Corollary 1.1.** When  $|\phi| < 1$ ,

$$\begin{aligned}
E(z_t|\phi) &= E\left(\sum_{h=0}^{\infty} z_{t,h}|\phi\right) = \sum_{h=0}^{\infty} E(z_{t,h}|\phi) = 0 \\
var(z_t|\phi) &= var\left(\sum_{h=0}^{\infty} z_{t,h}|\phi\right) = \sum_{h=0}^{\infty} var(z_{t,h}|\phi) = \sum_{h=0}^{\infty} \pi^2 \phi^{2h} = \frac{\pi^2}{1 - \phi^2}
\end{aligned}$$

Characteristic function of  $z_{h,t}$  is  $sech(\pi\phi^h t)$ . Thus, the characteristic function,  $g(t)$ , for  $\sum_{h=0}^{\infty} z_{h,t}$ , would be an infinite product of the characteristic function of  $z_{h,t}$ .

$$g(t) = \prod_{h=0}^{\infty} sech(\pi\phi^h t) \quad -\frac{1}{2} < t < \frac{1}{2}$$

Similarly, for the Moment Generating function  $M(t)$

$$M(t) = \prod_{h=0}^{\infty} sec(\pi\phi^h t) \quad -\frac{1}{2} < t < \frac{1}{2}$$

**Theorem 2.** If  $|\phi| = 0.5$ ,  $\eta_{t-h} \stackrel{iid}{\sim} Z(1/2, 1/2, 0, 1)$ , and  $z_{t,h} := \phi^h \eta_{t-h}$ , then  $z_t := \sum_{h=0}^{\infty} z_{t,h} \xrightarrow{a.s.} Logistic(0, 2)$ .

*Proof.* Derivations are explored in Appendix A.2. □

Thus, assuming  $\mu = 0$  and  $\phi = 0.5$  for simplicity, we have the following density function

for  $v_t$ ,  $\lambda_t := \exp\{v_t/2\}$  and  $\kappa_t := \frac{1}{1+\exp\{v_t\}}$  for the stationary distribution of DSP:

$$f(v_t) = \frac{1}{8} \operatorname{sech}^2\left(\frac{v_t}{4}\right)$$

$$f(\lambda_t) = \frac{1}{4\lambda_t} \operatorname{sech}^2\left(\frac{\log(\lambda_t)}{2}\right) = \frac{1}{(1+\lambda_t)^2}$$

$$f(\kappa_t) = \frac{1}{8(\kappa_t)(1-\kappa_t)} \operatorname{sech}^2\left(\frac{1}{4}\left(\log\left(\frac{1-\kappa_t}{\kappa_t}\right)\right)\right) = \frac{1}{\sqrt{\kappa_t(1-\kappa_t)}} \frac{1}{2\kappa_t(1+\sqrt{\frac{1-\kappa_t}{\kappa_t}})^2}.$$

Figure 2.4 compares the prior distribution of  $\lambda_t$  and  $\kappa_t$  for the Horseshoe and DSP. Let's

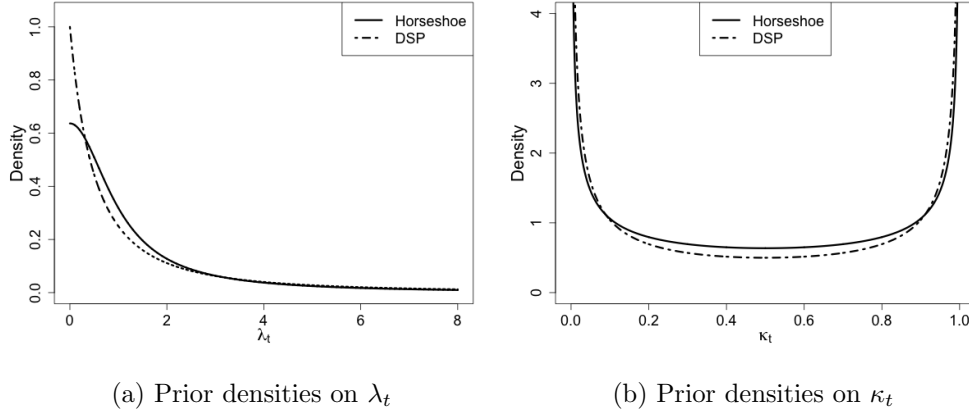


Figure 1: Comparisons of prior densities on  $\lambda_t$  and  $\kappa_t$  between Horseshoe Prior and the stationary distribution of Dynamic Shrinkage Process (DSP) with  $\eta_t \stackrel{iid}{\sim} Z(1/2, 1/2, 0, 1)$ ,  $\phi = 1/2$  and  $\mu = 0$ .

remind ourselves that the Horseshoe prior in Carvalho et al. [2010] assumes  $\lambda_t \sim C^+(0, 1)$  and  $\kappa_t \sim \text{Beta}(1/2, 1/2)$ . The density function for Horseshoe,  $g(\lambda_t)$  and  $g(\kappa_t)$  are:

$$g(\lambda_t) = \frac{2}{\pi(1+\lambda_t^2)} \quad g(\kappa_t) = \frac{1}{\pi\sqrt{\kappa_t(1-\kappa_t)}}.$$

For  $\lambda_t$ , the density function for DSP puts more weights as  $\lambda_t \rightarrow 0$  and  $\lambda_t \rightarrow \infty$ . Specifically,  $f(\lambda_t) > g(\lambda_t)$  when  $\lambda_t \in (0, \frac{2-\sqrt{(4-\pi)\pi}}{(\pi-2)}) \cup (\frac{2+\sqrt{(4-\pi)\pi}}{(\pi-2)}, \infty)$ . In terms of  $\kappa_t$ , the DSP puts

more weight around 0 and 1 than Horseshoe. This is due to the extra U-shaped term in  $\kappa_t$ ,  $\frac{1}{2\kappa_t(1+\sqrt{\frac{1-\kappa_t}{\kappa_t}})^2}$ , pushing the mass of the distribution to near 0 and 1. Let's consider the marginal density on  $\Delta h$ .

**Theorem 3.** Let  $|\phi| = 0.5$ ,  $\eta_{t-h} \stackrel{iid}{\sim} Z(1/2, 1/2, 0, 1)$ ,  $z_{t,h} := \phi^h \eta_{t-h}$ ,  $v_t := \sum_{h=0}^{\infty} z_{t,h}$ ,  $\lambda_t :=$

$\exp\{v_t/2\}$  and  $\Delta h_t \sim N(0, \lambda_t)$ ,

$$\lim_{\Delta h_t \rightarrow 0} f(\Delta h_t) = \infty$$

$$K_L \log\left(1 + \frac{4}{\Delta^2 h_t}\right) < f(\Delta h_t) < K_U \log\left(1 + \frac{2}{\Delta^2 h_t}\right), \quad |\Delta h_t| > 0$$

where  $K_U = \frac{1}{2\sqrt{2\pi}}$  and  $K_L = \frac{1}{8\sqrt{2\pi}}$

*Proof.* The proof is similar to Theorem 1 in Carvalho et al. [2010]. We use the fact that  $\forall x > 0$ ,

$$\frac{1}{2(1+x^2)} \leq \frac{1}{(1+x)^2} \leq \frac{1}{(1+x^2)}$$

Derivation is detailed in Appendix A.3. □

The bounds for the marginal distribution of DSP are similar to the ones from the Horseshoe with the only difference being the constant factor  $K_L$  and  $K_U$ . Under Horseshoe,  $K_U = \frac{1}{\sqrt{2\pi^3}}$  and  $K_L = \frac{1}{2\sqrt{2\pi^3}}$ . Like horseshoe prior, DSP is also unbounded near the origin, which leads to super-efficiency in a sparse setting as shown in Carvalho et al. [2010].

## 2.5 Jointly Modeling Both Trends in Mean and Variance

Finally, we propose Bayesian Trend Filter with Adaptive Stochastic Volatility (BTF-ASV) by combining Bayesian Trend Filter with Dynamic Horseshoe Process (BTF-DHP) proposed in Kowal et al. [2019] and ASV model proposed in this paper. BTF-ASV is able to generate smooth and locally adaptive estimate of the time varying mean parameter  $\beta_t$  through the Bayesian Trend Filter, and the time varying log variance parameter  $h_t$  via ASV, simultaneously.

Let's define  $\omega_{\beta,t} := \Delta^k \beta_t$  and also similarly define for variables  $v_{\beta,t}, u_{\beta,t}, \mu_{\beta}, \phi_{\beta}, \eta_{\beta,t}$  as well as for hyper-parameters  $a_{\eta_{\beta}}, b_{\eta_{\beta}}, a_{\mu_{\beta}}, b_{\mu_{\beta}}, a_{\phi_{\beta}}, b_{\phi_{\beta}}$ . We have the following Bayesian

hierarchical representation of BTF-ASV:

$$y_t = \beta_t + \exp\{h_t/2\}\epsilon_t \quad \epsilon_t \stackrel{iid}{\sim} N(0, 1) \quad (1a)$$

$$\Delta^k \beta_t = \omega_{\beta,t} = \exp\{v_{\beta,t}/2\}u_{\beta,t} \quad u_{\beta,t} \stackrel{iid}{\sim} N(0, 1) \quad (1b)$$

$$v_{\beta,t+1} = \mu_\beta + \phi_\beta(v_{\beta,t} - \mu_\beta) + \eta_{\beta,t} \quad \eta_{\beta,t} \stackrel{iid}{\sim} Z(a_{\eta_\beta}, b_{\eta_\beta}, 0, 1) \quad (1c)$$

$$\mu_h \sim Z(a_{\mu_\beta}, b_{\mu_\beta}, 0, 1) \quad (\phi_\beta + 1)/2 \sim \text{Beta}(a_{\phi_\beta}, b_{\phi_\beta}) \quad (1d)$$

$$\Delta^k h_t = \omega_{h,t} = \exp\{v_{h,t}/2\}u_{h,t} \quad u_{h,t} \stackrel{iid}{\sim} N(0, 1) \quad (1e)$$

$$v_{h,t+1} = \mu_h + \phi_h(v_{h,t} - \mu_h) + \eta_{h,t} \quad \eta_{h,t} \stackrel{iid}{\sim} Z(a_{\eta_h}, b_{\eta_h}, 0, 1) \quad (1f)$$

$$\mu_h \sim Z(a_{\mu_h}, b_{\mu_h}, 0, 1) \quad (\phi_h + 1)/2 \sim \text{Beta}(a_{\phi_h}, b_{\phi_h}) \quad (1g)$$

Line 1a represents the observation equation, lines 1b through 1d specify the priors on the time varying mean,  $\beta_t$  and lines 1e through 1g specify the priors on the time varying log-variance,  $h_t$ . Application of BTF-ASV is explored in Section 6.

### 3 Parameter Estimation

In this section, we explore estimation of ASV model. Let's remind ourselves that ASV has the following hierarchical representation:

$$y_t = \exp\{h_t/2\}\epsilon_t \quad \epsilon_t \stackrel{iid}{\sim} N(0, 1) \quad (2a)$$

$$\Delta^k h_t = \omega_t = \exp\{v_t/2\}u_t \quad u_t \stackrel{iid}{\sim} N(0, 1) \quad (2b)$$

$$v_{t+1} = \mu + \phi(v_t - \mu) + \eta_t \quad \eta_t \stackrel{iid}{\sim} Z(a_\eta, b_\eta, 0, 1). \quad (2c)$$

$$\mu \sim Z(a_\mu, a_\mu, 0, 1) \quad (\phi + 1)/2 \sim \text{Beta}(a_\phi, b_\phi), \quad (2d)$$

where  $a_\eta, b_\eta, a_\mu, a_\mu, a_\phi$ , and  $b_\phi$  are hyperparameters. Define  $\mathbf{y} := (y_1, \dots, y_T)'$ ,  $\mathbf{h} := (h_1, \dots, h_T)'$ , and  $\mathbf{v} := (v_1, \dots, v_T)'$ . The goal is to sample from the posterior distribution,  $f(\mathbf{h}, \mathbf{v}, \mu, \phi | \mathbf{y})$ . This may be achieved using Gibbs sampling, in which full conditional distribution for each variables,  $\mathbf{h}, \mathbf{v}, \mu$ , and  $\phi$  are sampled sequentially.

### 3.1 Parameter Expansion for the Likelihood

The difficulty in estimating the time-varying log-variance term  $h_t$  in SV model is its non-linear dependence in the likelihood. Sequential Monte Carlo by Jacquier et al. [1994] proposes sampling  $h_t$  sequentially, conditional on the past and future value of  $h_t$ . However, this method is indeed computationally intensive. Instead, we define  $y_t^* := \log(y_t^2)$ , and  $\mathbf{y}^* := (y_1^*, \dots, y_T^*)'$ , so that the model becomes linear system of equations with an unusual error term:

$$y_t^* = h_t + \log(\epsilon_t^2) \quad \epsilon_t \stackrel{iid}{\sim} N(0, 1).$$

We use the 10-component mixture Gaussian distribution by Omori et al. [2007] to approximate the non-Gaussian error term  $\epsilon_t^*$ :

$$y_t^* \approx h_t + \mu_{j_t} + \sigma_{j_t} o_t \quad o_t \stackrel{iid}{\sim} N(0, 1), \quad j_t \stackrel{iid}{\sim} \text{Categorical}(\pi)$$

The exact distribution for  $\pi$  can be found in Omori et al. [2007]. Conditional on the mixture component,  $j_t$ ,  $y_t^*$  is approximately a linear Gaussian State Space model where fast sampling of  $h_t$  becomes possible using the Cholesky factorization method proposed by Rue [2002]. Similarly, the change of variable and approximation is performed on  $\omega_{h,t}^* := \log(\omega_{h,t}^2) = \log((\Delta^k h_t)^2)$  when estimating the log-variance parameters for BTF-ASV model.

### 3.2 Parameter Expansion for the Z-distribution

Lines 2c and 2d of Model 3 can be viewed as SV model, with an exception that  $\eta_t \sim Z(a_\eta, b_\eta, 0, 1)$ , instead of  $N(0, 1)$ . Using the mean-variance scale mixture representation of the Z-distribution as explored in Barndorff-Nielsen et al. [1982]:

$$\eta|\xi \sim N(\xi^{-1}(a_\eta - b_\eta)/2, \xi^{-1})$$

$$\xi \sim PG(a_\eta + b_\eta, 0)$$

$\xi \sim PG(b_\xi, c_\xi)$  is an infinite convolution of gamma random variables:

$$\xi \stackrel{D}{=} (2\pi^2)^{-1} \sum_{k=1}^{\infty} g_k \left\{ \left(k - \frac{1}{2}\right)^2 - c_\xi^2 / (4\pi^2)^{-1} \right\},$$

where,  $g_k \stackrel{iid}{\sim} \text{gamma}(b_\xi, 1)$  and  $\stackrel{D}{=}$  indicates equality of distribution. Efficient sampling from Pólya-Gamma random variable is done via truncating an infinite sum as proposed by Polson et al. [2013]. With the parameter expansion, we may use efficient AWOL sampler proposed by Kastner and Frühwirth-Schnatter [2014] for sampling  $\mathbf{v}, \mu$  and  $\phi$ .

### 3.3 Gibbs Sampling with Parameter Expansion

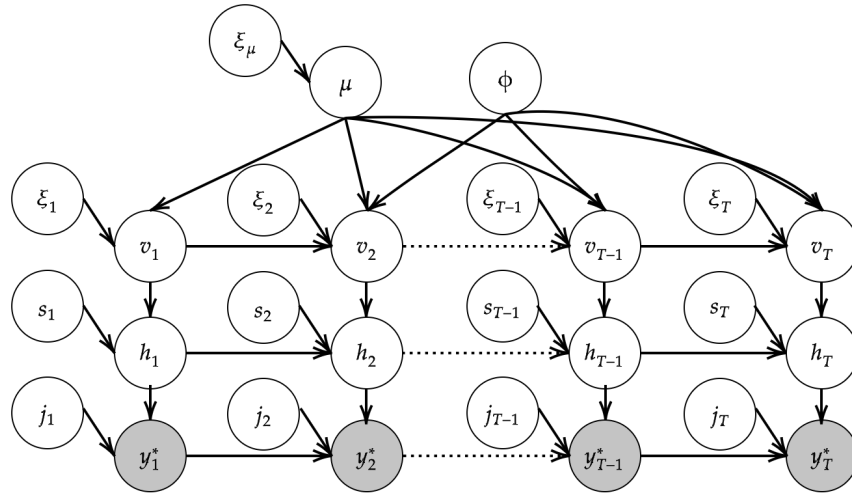


Figure 2: Graphical representations of Adaptive Stochastic Volatility with parameter expansions. In addition to the existing parameters,  $(\mathbf{h}, \mathbf{v}, \mu, \phi)$ , parameters  $(\mathbf{j}, \mathbf{s}, \boldsymbol{\xi}, \xi_\mu)$  are introduced for efficient Gibbs sampling.

Based on the approximations and parameter expansions explored in previous subsections, we have the following equation for ASV with Dynamic Horseshoe Priors (ASV-DHS)

with  $a_\eta = b_\eta = a_\mu = b_\mu = 1/2$ :

$$\begin{aligned}
y_t^* &\approx h_t + \mu_{j_t} + \sigma_{j_t} o_t & o_t &\stackrel{iid}{\sim} N(0, 1) \\
\Delta^k h_t = \omega_t^* &\approx v_t + \mu_{s_t} + \sigma_{s_t} r_t & r_t &\stackrel{iid}{\sim} N(0, 1) \\
v_{t+1} &= \xi_\mu^{-1/2} \mu + \phi(v_t - \mu) + \xi_t^{-1/2} \eta_t & \eta_t &\stackrel{iid}{\sim} N(0, 1) \\
\mu &\sim N(0, 1) & \xi_\mu &\stackrel{iid}{\sim} PG(1, 0) \\
\xi_t &\stackrel{iid}{\sim} N(0, 1) & s_t &\stackrel{iid}{\sim} Categorical(\pi) \\
j_t &\stackrel{iid}{\sim} Categorical(\pi) & & (\phi_h + 1)/2 \sim Beta(a_\phi, b_\phi).
\end{aligned}$$

In addition to the four parameters in the original equation,  $\mathbf{h}$ ,  $\mathbf{v}$ ,  $\mu$ , and  $\phi$ , four additional parameters,  $\mathbf{j} := (j_1, \dots, j_T)'$ ,  $\mathbf{s} := (s_1, \dots, s_T)'$ ,  $\boldsymbol{\xi} := (\xi_1 \dots \xi_T)'$ , and  $\xi_\mu$  are introduced via parameter expansion and approximation.

Graphical representation ASV with parameter expansion is illustrated in Figure 2. Define  $\theta^{1:T} = (\mathbf{j}, \mathbf{h}, \mathbf{v}, \mathbf{s}, \boldsymbol{\xi}, \mu, \xi_\mu, \phi)$  and  $\theta_{-j}^{1:T} = (\mathbf{h}, \mathbf{v}, \mathbf{s}, \boldsymbol{\xi}, \mu, \xi_\mu, \phi)$ . Similarly, define  $\theta_{-h}^{1:T}$  and so forth in a similar manner for all other variables. The following is the list of conditional distributions for Gibbs sampling. Despite the large number of parameters, many of the variables are conditionally independent, allowing efficient sampling scheme. The full conditional posterior distributions for Gibbs sampling are rigorously detailed in the supplementary material. Other than  $\phi$ , the closed form full conditional distribution was used.



Slice sampling by Neal [2003] were used for sampling  $\phi_h$ .

$$f(\mathbf{j}|\theta_{-j}^{1:T}, \mathbf{y}^*) = f(\mathbf{j}|\mathbf{h}, \mathbf{y}^*)$$

$$f(\mathbf{h}|\theta_{-h}^{1:T}, \mathbf{y}^*) = f(\mathbf{h}|\mathbf{j}, \mathbf{v}, \mathbf{s}, \mathbf{y}^*)$$

$$f(\mathbf{v}|\theta_{-v}^{1:T}, \mathbf{y}^*) = f(\mathbf{v}|\mathbf{s}, \mathbf{h}, \mu, \phi, \boldsymbol{\xi})$$

$$f(\mathbf{s}|\theta_{-s}^{1:T}, \mathbf{y}^*) = f(\mathbf{s}|\mathbf{h}, \mathbf{v})$$

$$f(\boldsymbol{\xi}|\theta_{-\xi}^{1:T}, \mathbf{y}^*) = f(\boldsymbol{\xi}|\mathbf{v}, \mu, \phi)$$

$$f(\mu|\theta_{-\mu}^{1:T}, \mathbf{y}^*) = f(\mu|\mathbf{v}, \boldsymbol{\xi}, \xi_\mu, \phi)$$

$$f(\xi_\mu|\theta_{-\xi_\mu}^{1:T}, \mathbf{y}^*) = f(\xi_\mu|\mu)$$

$$f(\phi|\theta_{-\phi}^{1:T}, \mathbf{y}^*) = f(\phi|\mathbf{v}, \boldsymbol{\xi}, \mu)$$

For the posterior distribution  $f(\theta^{1:T} | \mathbf{y}^*)$ , each parameter is initialized appropriately and then sampled sequentially from the eight conditional distributions shown above until convergence. A similar Gibbs sampling approach is used for BTF-ASV.

## 4 Simulation Study

### 4.1 Set-up

Assessing volatility models is challenging because the true underlying volatility is unobserved. To address this, our simulation study compares the proposed ASV with established models: SV, MSSV, RWSV, GARCH, and MSGARCH. The comparison is based on three metrics: accuracy, empirical coverage, and the mean credible interval width. Accuracy is evaluated using the Mean Absolute Error (MAE):

$$MAE(\hat{\sigma}) = \frac{1}{T} \sum_{t=1}^T |\sigma_t - \hat{\sigma}_t|,$$

which measures the difference between the true volatility  $\sigma_t$  and the model estimate  $\hat{\sigma}_t$ .

For Frequentist methods, the point estimate is the maximum likelihood estimate, while for

<b>DGS1: SV with 1 Regime</b>	<b>DGS4: GARCH with 1 Regime</b>
$h_{t+1} = 3 + 0.8(h_t - 3) + 0.2u_t$	$\sigma_{t+1}^2 = 1 + 0.1y_t^2 + 0.5\sigma_t^2$
<b>DGS2: SV with 2 Regimes</b>	<b>DGS5: GARCH with 2 Regimes</b>
$h_{t+1} = m_{s_{t+1}} + 0.8(h_t - m_{s_t}) + 0.2u_t$ $m_{s_t} = \begin{cases} -10, & \text{if } s_t = 0. \\ 6, & \text{if } s_t = 1. \end{cases}$	$\sigma_{t+1}^2 = m_{s_{t+1}} + 0.15y_t^2 + \beta_{s_{t+1}}\sigma_t^2$ $m_{s_t} = \begin{cases} 8, & \text{if } s_t = 0. \\ 0.1, & \text{if } s_t = 1. \end{cases}$ $\beta_{s_{t+1}} = \begin{cases} 0.8, & \text{if } s_t = 0. \\ 0.3, & \text{if } s_t = 1. \end{cases}$
<b>DGS3: SV with 3 Regimes</b>	<b>DGS6: GARCH with 3 Regimes</b>
$h_{t+1} = m_{s_{t+1}} + 0.8(h_t - m_{s_t}) + 0.2u_t$ $m_{s_t} = \begin{cases} -10, & \text{if } s_t = 0. \\ -3, & \text{if } s_t = 1. \\ 3, & \text{if } s_t = 2. \end{cases}$	$\sigma_{t+1}^2 = m_{s_{t+1}} + 0.15y_t^2 + \beta_{s_{t+1}}\sigma_t^2$ $m_{s_t} = \begin{cases} 12, & \text{if } s_t = 0. \\ 8, & \text{if } s_t = 1. \\ 0.1, & \text{if } s_t = 2. \end{cases}$ $\beta_{s_{t+1}} = \begin{cases} 0.8, & \text{if } s_t = 0. \\ 0.5, & \text{if } s_t = 1. \\ 0.2, & \text{if } s_t = 2. \end{cases}$

Table 1: Detailed summary of Data Generating Schemes (DGS) for the simulation study. Define  $y_t = \sigma_t \epsilon_t$ ,  $\epsilon_t \stackrel{iid}{\sim} N(0,1)$ ,  $u_t \stackrel{iid}{\sim} N(0,1)$ ,  $h_t := \log(\sigma_t^2)$ . Sample paths were generated from the stochastic volatility model with 1, 2, and 3 regimes for DGS 1, 2, and 3, respectively, and from the GARCH model with 1, 2, and 3 regimes for DGS 4, 5, and 6, respectively. Transitions between states 0 and 1 for DGS 2 and DGS 4 are governed by the following transition matrix  $\begin{pmatrix} 0.98 & 0.02 \\ 0.02 & 0.98 \end{pmatrix}$ . Transitions between states 0, 1 and 2 for DGS 3 and DGS 6 are governed by  $\begin{pmatrix} 0.98 & 0.01 & 0.01 \\ 0.01 & 0.98 & 0.01 \\ 0.01 & 0.01 & 0.98 \end{pmatrix}$ . Each DGS comprises 1,000 sample paths, each path being 1000 data points in length. Parameters for each DGS are detailed above.

Bayesian methods, it's the posterior mean. Empirical coverage:

$$\frac{1}{T} \sum_{t=1}^T 1_{(\hat{\sigma}_t, 0.05, \hat{\sigma}_t, 0.95)}(\sigma_t),$$

measures how often the true volatility falls within the 90% credible interval, reflecting the accuracy of each model's uncertainty quantification. Finally, the Mean Credible Interval

Width (MCIW):

$$\frac{1}{T} \sum_{t=1}^T (\hat{\sigma}_{t,0.95} - \hat{\sigma}_{t,0.05}),$$

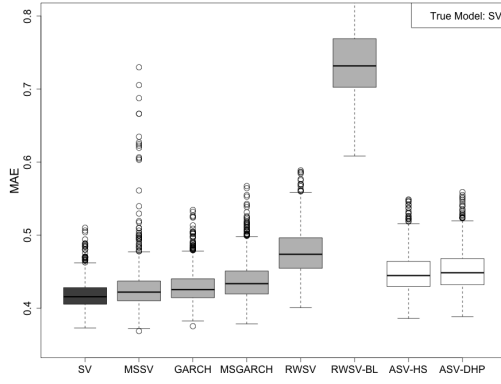
assesses the precision of the uncertainty quantification, where a narrower credible interval indicates better precision.

We generate 1,000 sample paths with 1,000 data points each for six DGSs outlined in Table 1. Note that SV, MSSV2, GARCH, and MSGARCH2 are the perfectly specified models for DGSs 1, 2, 4, and 5 respectively and are expected to perform the best in their respective DGSs. In DGS 3 and 6, none of the models are correctly specified. These scenarios test each model’s performance under misspecification.

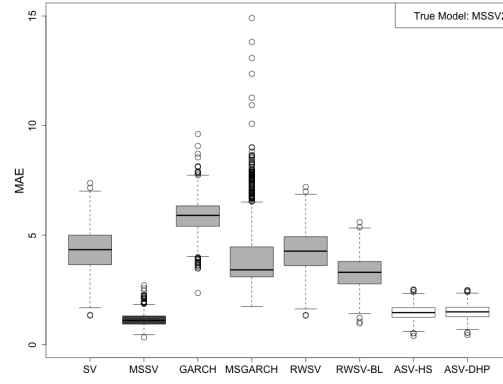
All models are implemented in R language (R Core Team [2013]). Specifically, SV model is implemented via `stochvol` (Kastner [2016]) package, MSSV2 as specified in Hamilton [1989] and RWSV are implemented by the authors as no readily available packages in R exists. GARCH(1,1) models are fitted via `fGarch` (Wuertz et al. [2023]) package, and MSSV2 are fitted via `MSGARCH` (Ardia et al. [2019]) package. For fitting RWSV-BL, `dsp` package by Kowal et al. [2019] and `genlasso` package by Arnold and Tibshirani [2022] are used. `dsp` package by Kowal et al. [2019] is further expanded to implement ASV models. For all Bayesian models, 5,000 posterior samples are generated after 20,000 burn-ins for each sample path.

## 4.2 Results

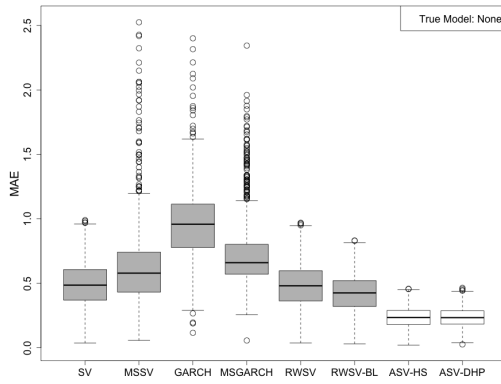
As shown in Figure 3, the SV, MSSV2, GARCH, and MSGARCH2 models achieve the lowest average MAE in DGSs 1, 2, 4, and 5, respectively, as they are the perfectly specified models for those scenarios. Both RWSV and RWSV-BL generally show similar or slightly lower accuracy compared to SV, with RWSV-BL offering only marginal improvements in DGSs 2, 3, 5, and 6, where volatility paths exhibit abrupt changes. Despite its design



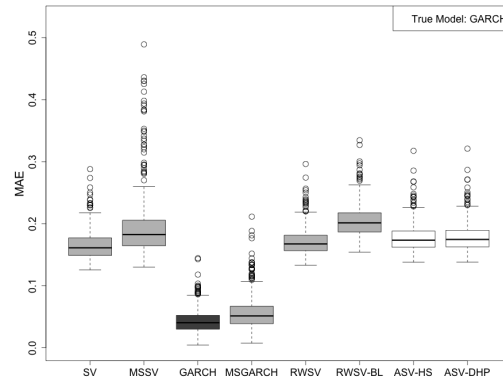
(a) DGS 1



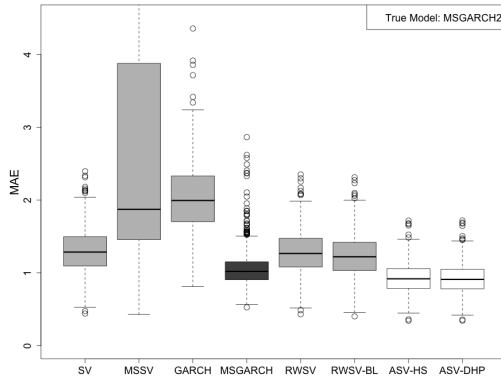
(b) DGS 2



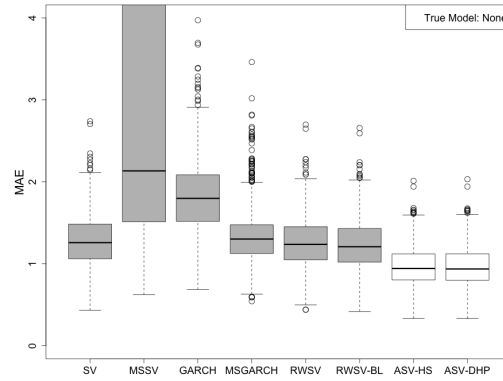
(c) DGS 3



(d) DGS 4



(e) DGS 5



(f) DGS 6

Figure 3: Box plots of Mean Absolute Error (MAE) across 1,000 sample paths comparing Stochastic Volatility (SV), Markov-Switching Stochastic Volatility with 2 Regimes (MSSV2), Generalized AutoRegressive Conditional Heteroskedasticity (GARCH), Markov-Switching GARCH with 2 regimes (MSGARCH2), Random Walk Stochastic Volatility with Inverse Gamma Prior (RWSV), Random Walk Stochastic Volatility with Bayesian LASSO (RWSV-BL), Adaptive Stochastic Volatility with Dynamic Horseshoe Prior (ASV-HS), and ASV with Dynamic Horseshoe Prior(ASV-DHS). Perfectly specified models, drawn in black, are SV and MSSV2 for DGS 1 and 2 and GARCH and MSGARCH2 for DGS 4 and 5, respectively. All models are misspecified for DGS 3 and 6.

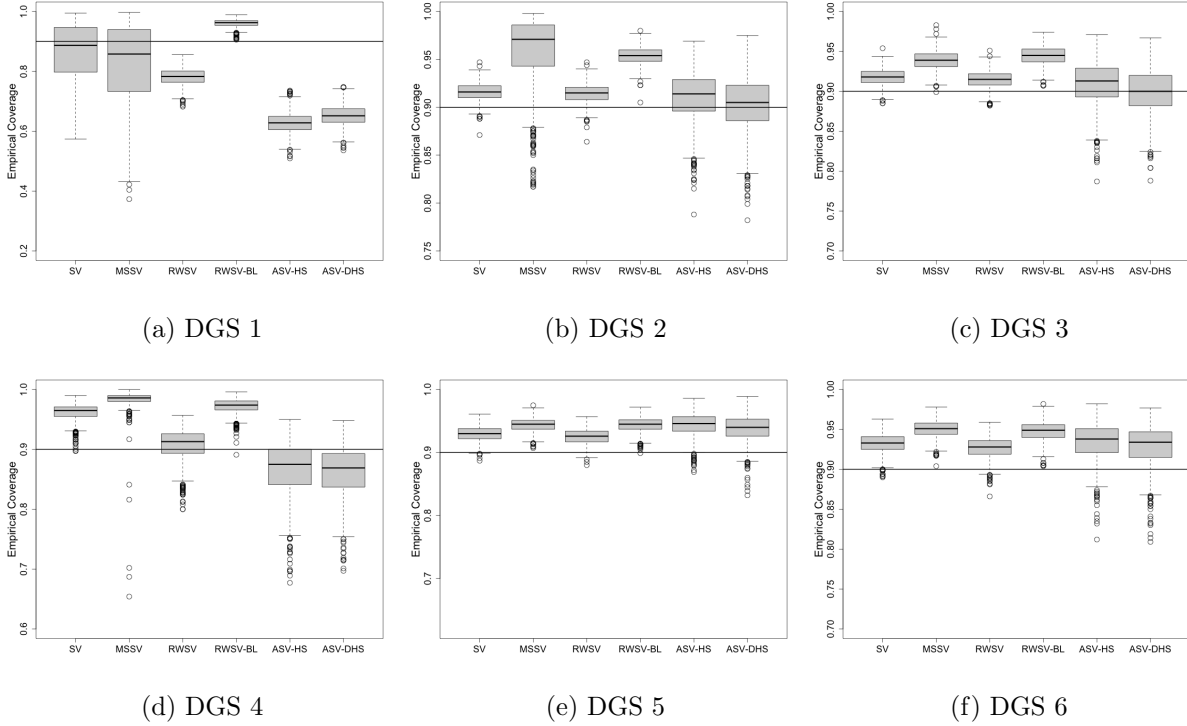


Figure 4: Box plots of empirical coverage of the 90% credible region across 1,000 sample paths of Bayesian methods: Stochastic Volatility (SV), Markov-Switching Stochastic Volatility with 2 Regimes (MSSV2), Random Walk Stochastic Volatility with Inverse Gamma Prior (RWSV), Random Walk Stochastic Volatility with Bayesian LASSO (RWSV-BL), Adaptive Stochastic Volatility with Dynamic Horseshoe Prior (ASV-HS), and ASV with Dynamic Horseshoe Prior(ASV-DHS). The horizontal line is drawn at the 90%.

for trend filtering, Bayesian LASSO does not provide a significant advantage in estimating time-varying volatility compared to its counterpart with a non-informative Inverse Gamma prior, underscoring the limitations of RWSV-BL.

The proposed ASV-HS and ASV-DHS models outperform or match the true models when large volatility shifts are present, as seen in DGSs 2, 3, 5, and 6. Their accuracy is only marginally lower than that of MSSV2 in DGS 2, and slightly higher than that of MSGARCH2 in DGS 5, which are the perfectly specified models for these cases. Additionally, ASV models significantly outperform all other models in DGSs 3 and 6, showcasing their strength in capturing volatility paths with abrupt changes. However, they are less effective in stationary volatility scenarios, such as in DGSs 1 and 4, likely due to the

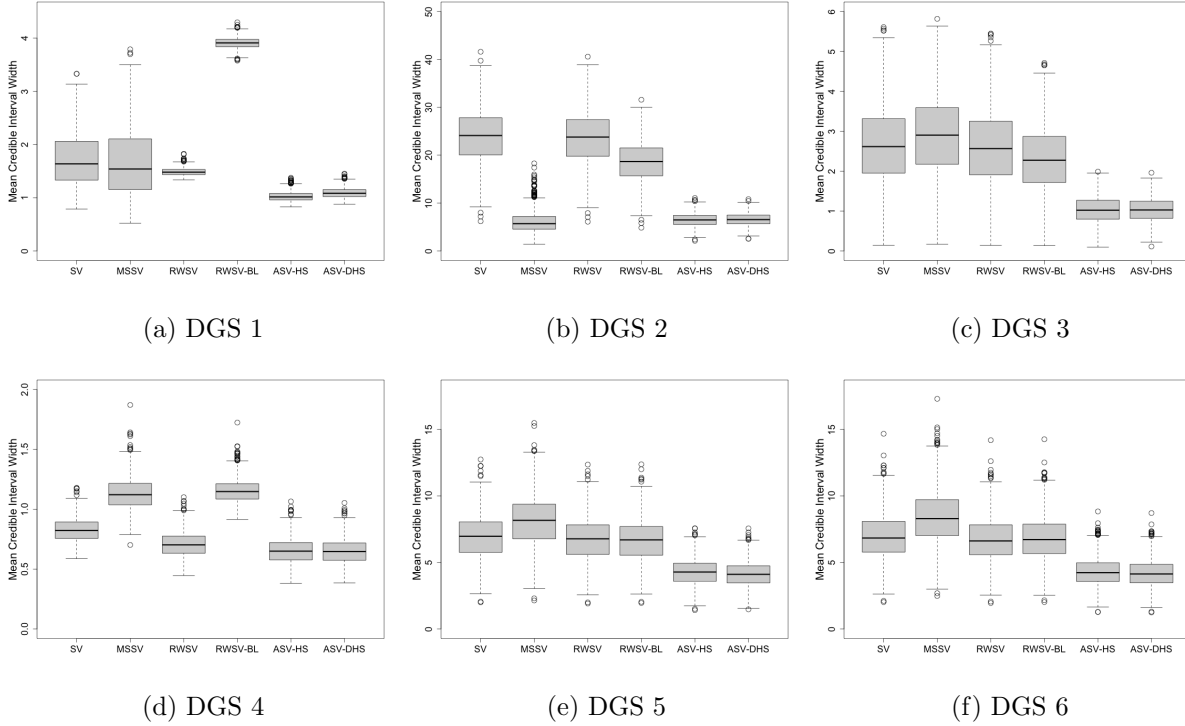


Figure 5: Box plots of mean credible interval widths of the 90% credible region across 1,000 sample paths of Bayesian methods: Stochastic Volatility (SV), Markov-Switching Stochastic Volatility (MSSV), Random Walk Stochastic Volatility with Inverse Gamma Prior (RWSV), Random Walk Stochastic Volatility with Bayesian LASSO (RWSV-BL), Adaptive Stochastic Volatility with Dynamic Horseshoe Prior (ASV-HS), and ASV with Dynamic Horseshoe Prior (ASV-DHS).

non-mean-reverting nature of the ASV model.

The simulation results further suggest that both Markov Switching models, MSSV2 and MSGARCH2, are less reliable than the ASV models. While they perform better on average in DGSs 1 and 4, their accuracy becomes highly variable when the assumed two-regime structure does not match the true underlying volatility process. For instance, if there is only one regime in the data, these models may produce inaccurate estimates by assigning non-zero probability to a non-existent second regime. This assumption occasionally leads to widely inconsistent estimating, resulting in high MAEs. In contrast, the ASV, which does not rely on a fixed regime structure, offers greater flexibility and more consistent performance across various volatility scenarios.

Figure 4 presents the empirical coverage of the 90% credible intervals for the six Bayesian methods in the simulation study: SV, MSSV2, RWSV, RWSV-BL, ASV-HS, and ASV-DHS. The existing models—SV, MSSV2, RWSV, and RWSV-BL—generally maintain reasonable nominal coverage across all DGSs. The proposed models, ASV-HS and ASV-DHS, also achieve correct nominal coverage (90%) in DGSs 2, 3, 5, and 6. However, they significantly underperform in DGS 1 and slightly underperform in DGS 4, likely due to their assumption of nonstationarity, which conflicts with the stationary volatility paths in those two cases.

Figure 5 illustrates the width of the 90% credible intervals, showing that the proposed models have the narrowest credible intervals across all DGSs. Maintaining a narrow credible interval while still achieving the correct coverage is a significant advantage, as it indicates both precise estimates and robust uncertainty quantification. In this respect, the proposed models outperform the existing ones in DGSs 2, 3, 5, and 6.

## 5 Empirical Study

### 5.1 Set-up

We apply ASV-DHS to empirical datasets and compare its volatility estimates with those from Stochastic Volatility (SV) and Random Walk Stochastic Volatility (RWSV) models. Specifically, we analyze the price of S&P500 from 2012-01-01 to 2021-12-31 ( $n = 1148$ , Figure 6a), EURO to US Dollar exchange rate between 2000-01-03 to 2012-04-04 ( $n = 639$ , Figure 6b), and new deaths from COVID-19 from 2020-01-03 to 2023-11-13 ( $n = 202$ , Figure 6c). ASV model is applied to the weekly log return series for S&P 500 and EURO/USD exchange (Figure 6d and Figure 6e), and the weekly first difference series for COVID-19 death tolls in the U.S. (Figure 6f).

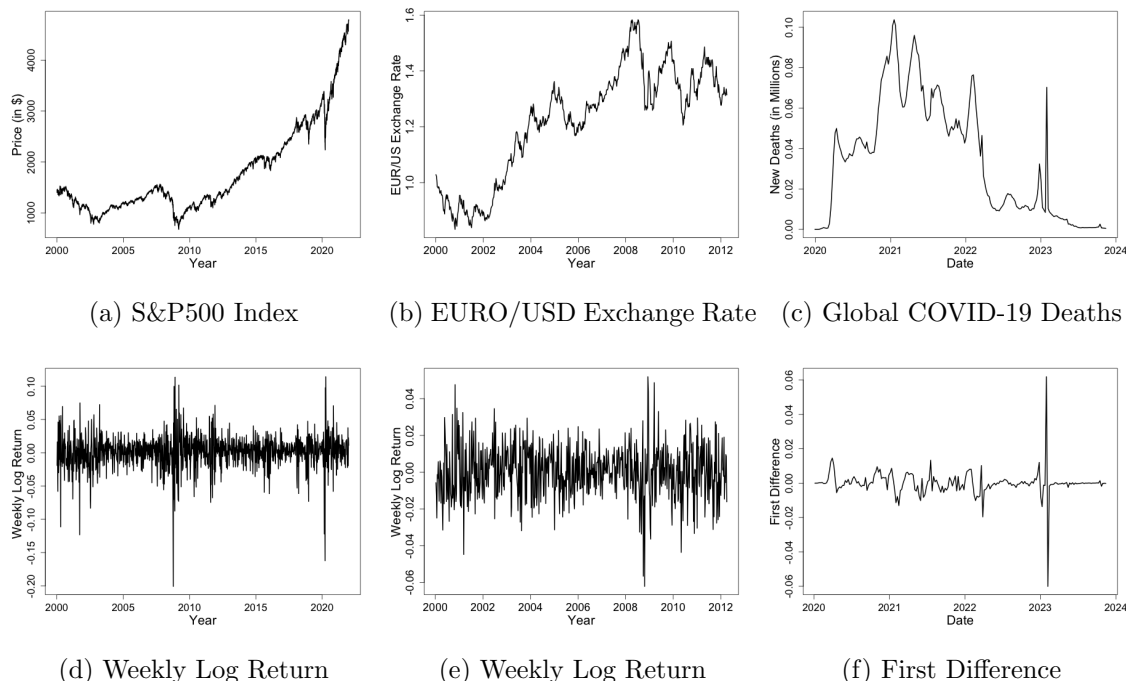


Figure 6: Price of S&P500 between 2012-01-01 and 2021-12-31 (a), EURO/USD exchange rate between 2000-01-03 and 2012-04-04 (b) and weekly COVID-19 new death tolls between 2020-01-03 to 2023-11-13 (c) in the United States are drawn. The weekly log return series for S&P500 and the exchange rate series are drawn in (d) and (e). The first difference series of COVID-19 death tolls are drawn in (f).

## 5.2 Results

We first assess the log-volatility ( $h_t$ ) estimates generated by ASV-DHS in comparison with RWSV and SV model across three data sets (Figure 7). Focusing on the S&P 500 dataset (Figures 7a, 7d and 7g), the most prominent features are the two large spikes in 2009 and 2020 due to financial crisis and COVID-19 outbreaks. In terms of moderate changes, the one around 2001 coincides with 9/11 attack and the 2011 surge aligns with the European Debt crisis, both of which caused a stock market decline. The stock market in 2018 followed the strongest 2017 market since the financial crisis but was overall exhibited extreme volatility, likely due to U.S. government shut down early and late in that year. While discernible in ASV, small to moderate changes in volatility is hard to distinguish from noise in noisier estimates from SV and RWSV.



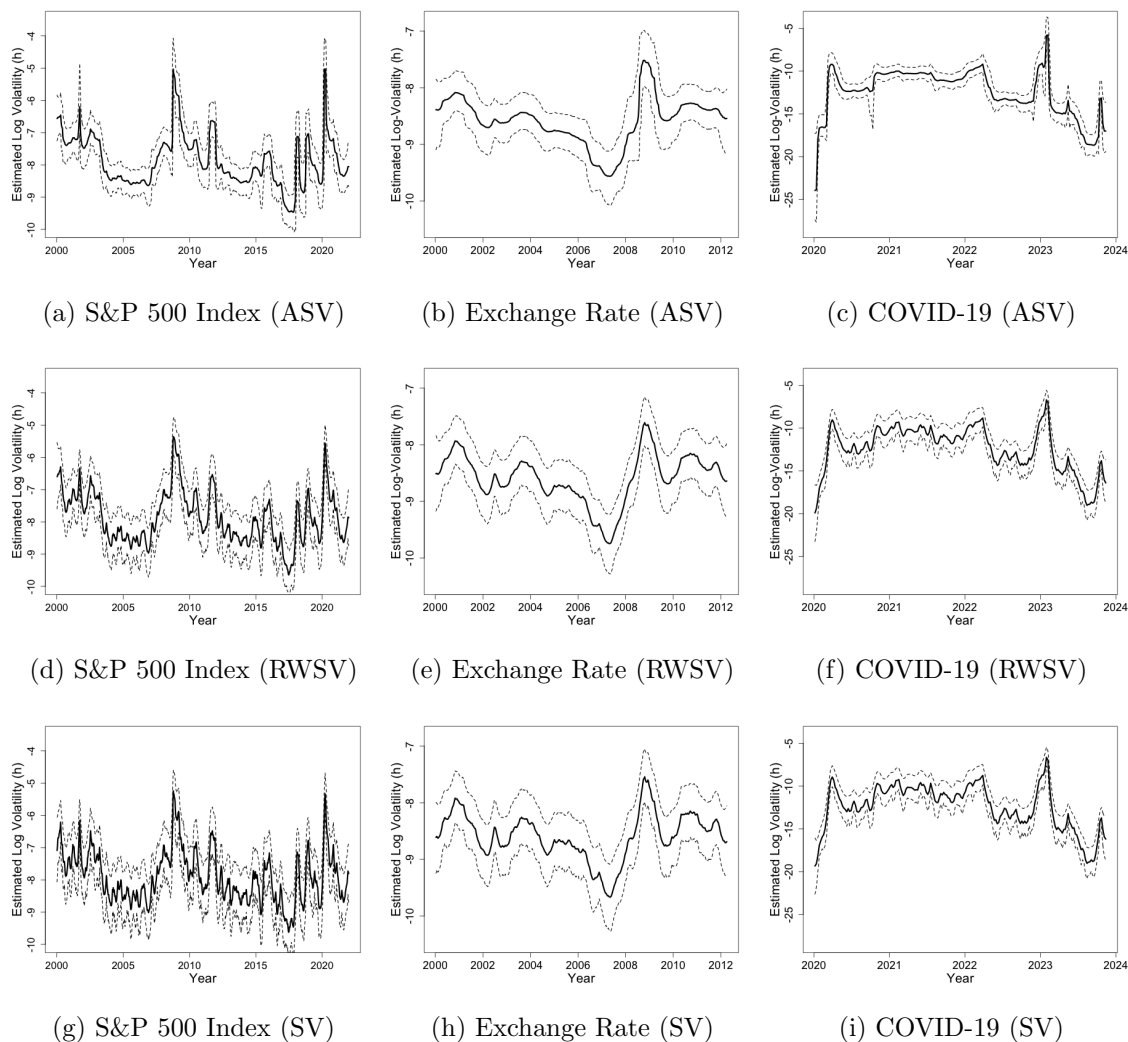


Figure 7: Estimated  $h$  with 90% quantile-based credible regions on weekly returns on S&P 500 between 2000-01-01 and 2021-12-31, weekly returns on EURO/USD exchange rate between 2000-01-03 and 2012-04-04, and weekly changes in COVID-19 death tolls in the U.S. between 2020-01-03 and 2023-11-13 based on Adaptive Shrinkage Process with Dynamic Shrinkage Process (ASV-DHS) shown in (a),(b), and (c), based on Random Walk Stochastic Volatility with inverse Gamma prior (RWSV) shown in (d), (e), and (f) and based on Stochastic Volatility (SV) model shown in (g),(h), and (i).

The EURO/USD exchange rate’s most notable volatility pattern includes a steady decline from 2001 to 2008, a substantial spike in 2008 and 2009 due to the financial crisis, and a minor bump in 2010 and 2011, likely tied to the European Debt crisis as well (Figures 7b, 7e and 7h). Figure 6b suggests a steady increase in the EURO/USD exchange rate between 2001 and 2008, resulting in low volatility. ASV, RWSV and SV all exhibit a very similar

pattern, with ASV displaying a smoother output than those of RWSV and SV. Because of this, The steady decline in volatility from 2001 to 2007 is easier to notice from ASV than from both SV and RWSV.

A discernible pattern from all three models for COVID-19 death tolls is the significant volatility spike occurring around the onset of the pandemic in early 2020 and another one in early 2023 (Figures 7c, 7f and 7i). Subsequently, seasonal effect appears to be present; there are small to large increases in volatility at the end and beginning of each year, followed by reductions in the summer months, particularly noticeable in 2022 and 2023. In mid-2022, a substantial dip in volatility is observed, succeeded by a notable spike toward the end of 2022 and the beginning of 2023. By the mid-2023, volatility plateaus, and experience dramatic decline, only to exhibit another spike by the end of 2023. This pattern is also observed to a lesser extent in 2020 and 2021, according to estimates from ASV. Such pattern is less noticeable based on estimates from both SV and RWSV.

All three models' estimates appear to share the same overall pattern, but with varying degree of smoothness. ASV generates the smoothest estimate out of the three models followed by RWSV and SV across the three data sets. A key advantage of this enhanced smoothness is improved interpretability. As discussed earlier, ASV-DHS excels, particularly in discerning small to medium changes in volatility, offering better clarity in distinguishing signal from noise compared to SV or RWSV, whose outputs tend to be noisier, rendering signals often indistinguishable from the noise. The reduced noise in ASV's output enables users to gain a clearer understanding of underlying patterns and trends.

Another distinguishing feature of ASV is its locally adaptive credible region. Due to time-varying variance term  $\tau\lambda_t = \exp\{v_t/2\}$ , credible region around  $h_t$  produced by ASV-DHS also changes over time. The mean-centered credible regions generated by SV, RWSV

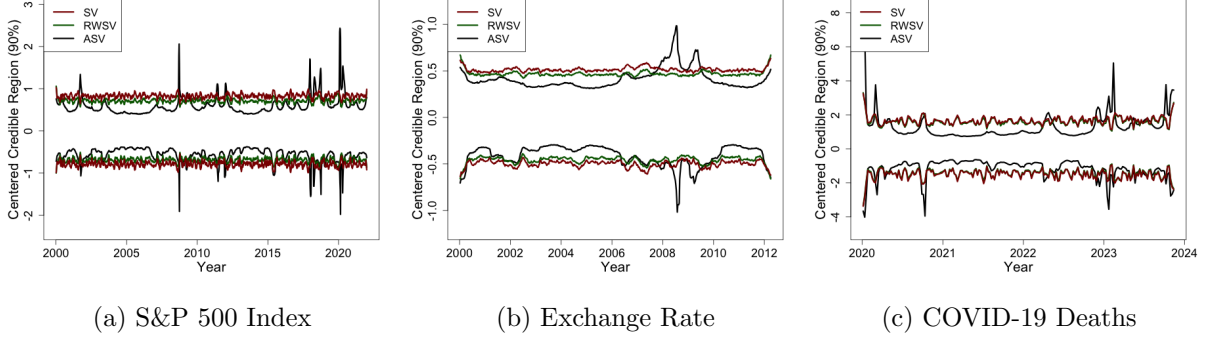


Figure 8: The 90% quantile-based credible regions on the log-variance  $h_t$  are subtracted by its posterior sample mean. The three datasets include weekly returns on S&P 500 between 2000-01-01 and 2021-12-31, weekly returns on EURO/USD exchange rate between 2000-01-03 and 2012-04-04, and weekly changes in COVID-19 death tolls between 2020-01-03 and 2023-11-13 in the U.S. The centered credible regions for Adaptive Stochastic Volatility with Dynamic Shrinkage Processes (ASV-DHS) are drawn in black, the ones based on Stochastic Volatility (SV) model are in dark red and the ones based on Random Walk Stochastic Volatility (RWSV) model are in dark green.

and ASV on the three data sets are illustrated in Figure 8. Notably, the credible regions maintain a constant width for both SV and RWSV model across the sample path with RWSV having slightly narrower credible region. The credible region around  $h$  for ASV, on the other hand, exhibits local adaptability. Specifically, the patterns on the centered credible regions match that of  $h_t$  explored in previous paragraphs. When changes in  $h_t$  are slow moving, the width of the credible region is narrow; while abrupt changes in  $h_t$  induce large credible regions.

Lastly, we analyze the empirical shrinkage parameter  $\kappa_t$ . The parameter  $v_t$  represents the log-variance term of  $\Delta h_t$ . A small  $v_t$  corresponds to minor changes in  $h_t$ , while a large  $v_t$  signifies substantial variations. Alternatively,  $v_t$  can be seen as influencing the degree of shrinkage applied to  $h_t$ , denoted as  $\kappa_t := \frac{1}{1+\text{var}(\omega_t|\tau, \lambda_t)} = \frac{1}{1+\exp(v_t)} = \frac{1}{1+\tau^2 \lambda_t^2}$ . Analyzing  $\kappa_t$  rather than  $v_t$  is preferred for clarity since  $\kappa_t \in (0, 1)$ , unlike  $v_t \in (-\infty, +\infty)$ . A high  $\kappa_t$  (near 1) indicates strong model certainty, while a low  $\kappa_t$  (near 0) indicates less certainty in the estimate. Figure 9 shows the comparison between the estimated log-volatility  $h_t$

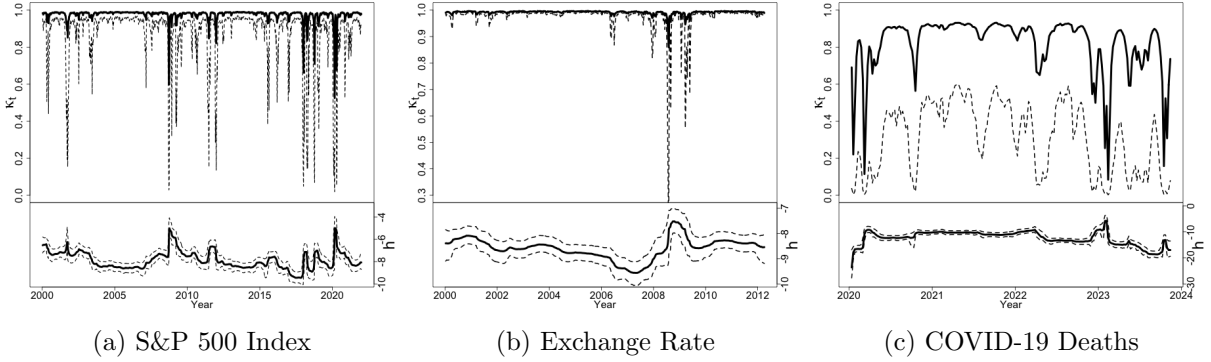


Figure 9: Comparison between the expected shrinkage parameter  $\kappa_t := \frac{1}{1+\text{var}(\omega_t|\tau, \lambda_t)} = \frac{1}{1+\text{exp}\{v_t\}} = \frac{1}{1+\tau^2\lambda_t^2}$  and expected  $h_t$  based on Adaptive Stochastic Volatility with Dynamic Horseshoe Prior (ASV-DHS) estimated on weekly returns on S&P 500 between 2000-01-01 and 2021-12-31, weekly returns on EURO/USD exchange rate between 2000-01-03 and 2012-04-04, and weekly changes in COVID-19 death tolls in the U.S. between 2020-01-03 and 2023-11-13, respectively. The dotted lines represent the one-sided 95th and centered 90th percentile credible regions for  $\kappa_t$  and  $h_t$  respectively.

and the shrinkage parameter  $\kappa_t$ . As expected in ASV, prominent peaks in  $h_t$  correspond to  $\kappa_t$  values near 0. During periods of gradual evolution,  $\kappa_t$  is close to 1. Generally,  $\kappa_t$  for the COVID-19 deaths data is more volatile than for the S&P 500 and exchange rate data, indicating lower certainty in the model’s estimates. This could be due to the smaller sample size of the COVID-19 dataset (203 data points) compared to the S&P 500 (1148 data points) and exchange rate (639 data points) datasets.

## 6 Trend Filtering Jointly in Mean and Variance

Kowal et al. [2019] applies the DSP to Dynamic Linear Model and refers to the model as Bayesian Trend Filter with Dynamic Shrinkage Processes (BTF-DSP). We extend BTF-DSP by incorporating ASV on its error process. The resulting model provide smooth yet locally adaptive estimate of both the mean process  $\beta_t$  and the log variance process  $h_t$ . Exact specification of the model is discussed in Model 1. In this section, we apply this method to analyze monthly global land surface air temperature anomaly with reference period 1951-1980 in 0.01 degree Celsius from 1880 to 2018. The data maybe found in this

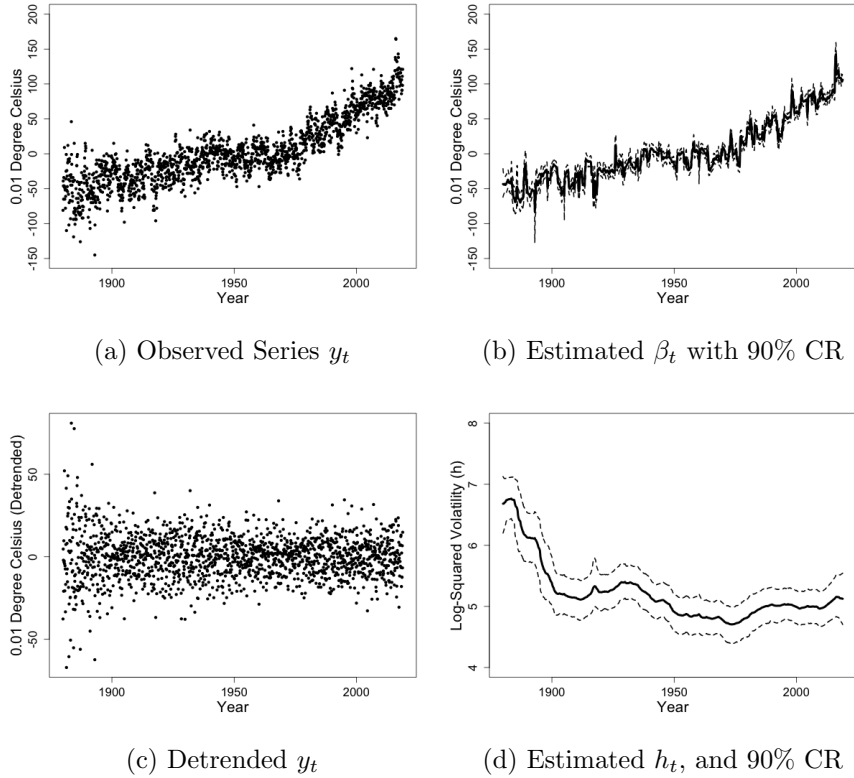


Figure 10: The monthly average global land surface air temperature anomaly from 1880 to 2018 with average temperature between 1950 and 1980 as base is illustrated in figure (a). Bayesian Trend Filter with Adaptive Stochastic Volatility is used to estimate the mean trend  $\beta_t$  and is illustrated in (b) with 90% credible region. Posterior mean for  $\beta_t$  was subtracted from the observed series to detrend the series and are illustrated in (c). BTF-ASV estimate of log-variance,  $h_t$  and its 90% credible regions is shown in (d).

url: [https://data.giss.nasa.gov/gistemp/taledata\\_v3/GLB.Ts.txt](https://data.giss.nasa.gov/gistemp/taledata_v3/GLB.Ts.txt).

The global temperature has demonstrated a consistent upward trend from 1880 to 2018 (Figure 6). This is reflected in the estimated posterior mean for  $\beta$ , showing a similar but smoother pattern. It is important to note that despite the model’s tendency to generate a smooth estimate, local trends still persist. This is likely attributed to yearly seasonal fluctuations as well large scale climate pattern such as El Niño and La Niña. Furthermore, there is a discernible shift in volatility over time. Notably, before 1900, extreme temperatures occurred more frequently, with wider range of fluctuations in temperature. Post-1900, however, temperatures remained within a narrower range, with occasional out-

liers. This pattern is captured by our estimation of log variance. The calculated volatility peaks around 1880 and gradually decreases until 1900. Subsequently, between 1900 and 2018, volatility appears to stabilize, as illustrated in Figure 6.

## 7 Conclusion

In this paper, we extend the RWSV model to create a flexible and adaptive framework for modeling time-varying volatility with both abrupt and gradual changes. Initially, we introduce RWSV-BL, incorporating the time-varying variance of  $\Delta h_t$  with a popular shrinkage prior, Bayesian LASSO. However, our simulation study reveals that RWSV-BL is suboptimal compared to existing models; we enhance RWSV-BL by applying a global-local shrinkage prior to the variance of  $\Delta h_t$ , leading to the development of ASV.

Using the global-local shrinkage prior introduced by Kowal et al. [2019], we develop two versions: ASV-HS and ASV-DHS. Extensive simulation studies show ASV demonstrates high accuracy, producing narrower credible intervals than the existing models while maintaining correct coverage, especially when the true volatility path exhibits large changes. Unlike Markov-Switching models, ASV does not require specifying the number of regimes and exhibits lower misspecification error. However, its performance declines when the volatility path is mean-reverting. ASV's ability to produce smooth yet locally adaptive estimates is also a big advantage as it offers more interpretable results.

Finally, we integrate ASV into the error process of the Bayesian Trend Filter proposed in Kowal et al. [2019], resulting in BTF-ASV. Empirical studies reveal its ability to produce smooth estimates of both time-varying mean and time-varying variance. Future research directions could explore the applications of ASV and DSP-ASV in diverse fields such as Finance, Environmental Science, and Epidemiology, leveraging their adaptability in modeling time-series exhibiting complex patterns.

## 8 Acknowledgement

Financial support from National Science Foundation grants OAC-1940124 and DMS-2114143 is gratefully acknowledged.

## 9 Supplementary Material

**Appendices:** A document including detailed proofs on the properties of Dynamic Shrinkage Processes (DSP) in section A, the exact prior distributions and detailed derivations of the full conditional distributions for Gibbs sampling in section B.

## References

- Jorge Achcar, Ricardo de Oliveira, and Emerson Barili. Use of stochastic volatility models in epidemiological data: Application to a dengue time series in são paulo city, brazil. *Journal of Biostatistics and Epidemiology*, 6(1):19–29, Oct. 2020. doi: 10.18502/jbe.v6i1.4755. URL <https://jbe.tums.ac.ir/index.php/jbe/article/view/338>.
- David Ardia, Keven Bluteau, Kris Boudt, and Leopoldo Catania. Forecasting risk with markov-switching garch models: A large-scale performance study. *International Journal of Forecasting*, 34(4):733–747, 2018.
- David Ardia, Keven Bluteau, Kris Boudt, Leopoldo Catania, and Denis-Alexandre Trotter. Markov-switching garch models in r: The msgarch package. *Journal of Statistical Software*, 91(4):1–38, 2019. doi: 10.18637/jss.v091.i04.
- Taylor B. Arnold and Ryan J. Tibshirani. *genlasso: Path Algorithm for Generalized Lasso Problems*, 2022. URL <https://CRAN.R-project.org/package=genlasso>. R package version 1.6.1.
- O. Barndorff-Nielsen, J. Kent, and M. Sørensen. Normal variance-mean mixtures and z distributions. *International Statistical Review / Revue Internationale de Statistique*, 50(2):145–159, 1982. ISSN 03067734, 17515823. URL <http://www.jstor.org/stable/1402598>.
- Luc Bauwens, Arie Preminger, and Jeroen V. K. Rombouts. Theory and inference for a markov switching garch model. *The Econometrics Journal*, 13(2):218–244, 2010. ISSN 13684221, 1368423X. URL <http://www.jstor.org/stable/23117467>.
- Anindya Bhadra, Jyotishka Datta, Nicholas G. Polson, and Brandon Willard. The horse-shoe+ estimator of ultra-sparse signals, 2015.
- Tim Bollerslev. Generalized autoregressive conditional heteroskedasticity. *Journal of Econometrics*, 31(3):307–327, 1986. ISSN 0304-4076. doi: [https://doi.org/10.1016/0304-4076\(86\)90063-1](https://doi.org/10.1016/0304-4076(86)90063-1). URL <https://www.sciencedirect.com/science/article/pii/0304407686900631>.
- Celso Brunetti, Chiara Scotti, Roberto S Mariano, and Augustine HH Tan. Markov switching garch models of currency turmoil in southeast asia. *Emerging Markets Review*, 9(2):104–128, 2008.
- Annalisa Cadonna, Sylvia Frühwirth-Schnatter, and Peter Knaus. Triple the gamma – a unifying shrinkage prior for variance and variable selection in sparse state space and tvp models, 2019.
- Jun Cai. A markov model of switching-regime arch. *Journal of Business & Economic Statistics*, 12(3):309–316, 1994. ISSN 07350015. URL <http://www.jstor.org/stable/1392087>.
- Guglielmo Maria Caporale and Timur Zekokh. Modelling volatility of cryptocurrencies using markov-switching garch models. *Research in International Business and Finance*, 48:143–155, 2019.
- CARLOS M. Carvalho, NICHOLAS G. POLSON, and JAMES G. SCOTT. The horseshoe estimator for sparse signals. *Biometrika*, 97(2):465–480, 2010. ISSN 00063444, 14643510. URL <http://www.jstor.org/stable/25734098>.
- Ray Yeutien Chou. Volatility persistence and stock valuations: Some empirical evidence using garch. *Journal of Applied Econometrics*, 3(4):279–294, 1988. ISSN 08837252, 10991255. URL <http://www.jstor.org/stable/2096644>.



- Michael J Dueker. Markov switching in garch processes and mean-reverting stock-market volatility. *Journal of Business & Economic Statistics*, 15(1):26–34, 1997.
- Robert F. Engle. Autoregressive conditional heteroscedasticity with estimates of the variance of united kingdom inflation. *Econometrica*, 50(4):987–1007, 1982. ISSN 00129682, 14680262. URL <http://www.jstor.org/stable/1912773>.
- Kenneth French, G. Schwert, and Robert Stambaugh. Expected stock returns and volatility. *Journal of Financial Economics*, 19(1):3–29, 1987. URL <https://EconPapers.repec.org/RePEc:eee:jfinec:v:19:y:1987:i:1:p:3-29>.
- Stephen F. Gray. Modeling the conditional distribution of interest rates as a regime-switching process. *Journal of Financial Economics*, 42(1):27–62, September 1996. URL <https://ideas.repec.org/a/eee/jfinec/v42y1996i1p27-62.html>.
- James D. Hamilton. A new approach to the economic analysis of nonstationary time series and the business cycle. *Econometrica*, 57(2):357–384, 1989. ISSN 00129682, 14680262. URL <http://www.jstor.org/stable/1912559>.
- James D Hamilton and Raul Susmel. Autoregressive conditional heteroskedasticity and changes in regime. *Journal of Econometrics*, 64(1):307–333, 1994. ISSN 0304-4076. doi: [https://doi.org/10.1016/0304-4076\(94\)90067-1](https://doi.org/10.1016/0304-4076(94)90067-1). URL <https://www.sciencedirect.com/science/article/pii/0304407694900671>.
- Andrew Harvey, Esther Ruiz, and Neil Shephard. Multivariate stochastic variance models. *The Review of Economic Studies*, 61(2):247–264, 04 1994. ISSN 0034-6527. doi: 10.2307/2297980. URL <https://doi.org/10.2307/2297980>.
- Florian Huber and Michael Pfarrhofer. Dynamic shrinkage in time-varying parameter stochastic volatility in mean models. *Journal of Applied Econometrics*, 36(2):262–270, 2021. doi: <https://doi.org/10.1002/jae.2804>. URL <https://onlinelibrary.wiley.com/doi/abs/10.1002/jae.2804>.
- JOHN Hull and ALAN White. The pricing of options on assets with stochastic volatilities. *The Journal of Finance*, 42(2):281–300, 1987. doi: <https://doi.org/10.1111/j.1540-6261.1987.tb02568.x>. URL <https://onlinelibrary.wiley.com/doi/abs/10.1111/j.1540-6261.1987.tb02568.x>.
- Soosung Hwang, Steve E. Satchell, and Pedro L. Valls Pereira. How Persistent is Volatility? An Answer with Stochastic Volatility Models with Markov Regime Switching State Equations. Econometric Society 2004 Latin American Meetings 198, Econometric Society, August 2004. URL <https://ideas.repec.org/p/ecm/latm04/198.html>.
- Eric Jacquier, Nicholas G. Polson, and Peter E. Rossi. Bayesian analysis of stochastic volatility models. *Journal of Business & Economic Statistics*, 12(4):371–389, 1994. ISSN 07350015. URL <http://www.jstor.org/stable/1392199>.
- Gregor Kastner. Dealing with stochastic volatility in time series using the R package stochvol. *Journal of Statistical Software*, 69(5):1–30, 2016. doi: 10.18637/jss.v069.i05.
- Gregor Kastner and Sylvia Frühwirth-Schnatter. Ancillarity-sufficiency interweaving strategy (ASIS) for boosting MCMC estimation of stochastic volatility models. *Computational Statistics & Data Analysis*, 76:408–423, aug 2014. doi: 10.1016/j.csda.2013.01.002. URL <https://doi.org/10.1016%2Fj.csda.2013.01.002>.
- Seung-Jean Kim, Kwangmoo Koh, Stephen Boyd, and Dimitry Gorinevsky.  $l_1$  trend filtering. *SIAM Rev.*, 51(2):339–360, 2009. ISSN 0036-1445,1095-7200. doi: 10.1137/070690274. URL <https://doi.org/10.1137/070690274>.

- Polychronis Kostoulas, Eletherios Meletis, Konstantinos Pateras, Paolo Eusebi, Theodoros Kostoulas, Luis Furuya-Kanamori, Niko Speybroeck, Matthew Denwood, Suhail Doi, Christian Althaus, Carsten Kirkeby, Pejman Rohani, Navneet Dhand, José Peñalvo, Lehana Thabane, Ben miled Slimane, Hamid Sharifi, and Stephen Walter. The epidemic volatility index, a novel early warning tool for identifying new waves in an epidemic. *Scientific Reports*, 11:23775, 12 2021. doi: 10.1038/s41598-021-02622-3.
- Daniel R. Kowal, David S. Matteson, and David Ruppert. Dynamic Shrinkage Processes. *Journal of the Royal Statistical Society Series B: Statistical Methodology*, 81(4):781–804, 05 2019. ISSN 1369-7412. doi: 10.1111/rssb.12325. URL <https://doi.org/10.1111/rssb.12325>.
- Jiaxin Ma, Feiyun Xu, Kai Huang, and Ren Huang. Gnar-garch model and its application in feature extraction for rolling bearing fault diagnosis. *Mechanical Systems and Signal Processing*, 93:175–203, 2017.
- Saeid Mehdizadeh, Javad Behmanesh, and Keivan Khalili. A comparison of monthly precipitation point estimates at 6 locations in iran using integration of soft computing methods and garch time series model. *Journal of Hydrology*, 554:721–742, 2017. ISSN 0022-1694. doi: <https://doi.org/10.1016/j.jhydrol.2017.09.056>. URL <https://www.sciencedirect.com/science/article/pii/S0022169417306601>.
- Angelo Melino and Stuart M. Turnbull. Pricing foreign currency options with stochastic volatility. *Journal of Econometrics*, 45(1-2):239–265, 1990. URL <https://EconPapers.repec.org/RePEc:eee:econom:v:45:y:1990:i:1-2:p:239-265>.
- Reza Modarres and Taha BMJ Ouarda. Modeling the relationship between climate oscillations and drought by a multivariate garch model. *Water Resources Research*, 50(1):601–618, 2014.
- Radford M. Neal. Slice sampling. *The Annals of Statistics*, 31(3):705 – 767, 2003. doi: 10.1214/aos/1056562461. URL <https://doi.org/10.1214/aos/1056562461>.
- Haruhisa Nishino and Kazuhiko Kakamu. A random walk stochastic volatility model for income inequality. *Japan and the World Economy*, 36:21–28, 2015. ISSN 0922-1425. doi: <https://doi.org/10.1016/j.japwor.2015.06.003>. URL <https://www.sciencedirect.com/science/article/pii/S0922142515000328>.
- Yasuhiro Omori, Siddhartha Chib, Neil Shephard, and Jouchi Nakajima. Stochastic volatility with leverage: Fast and efficient likelihood inference. *Journal of Econometrics*, 140(2):425–449, 2007. ISSN 0304-4076. doi: <https://doi.org/10.1016/j.jeconom.2006.07.008>. URL <https://www.sciencedirect.com/science/article/pii/S0304407606001436>.
- Martins Otache. Conditional heteroscedasticity in streamflow process: Paradox or reality? *Open Journal of Modern Hydrology*, 02:79–90, 01 2012. doi: 10.4236/ojmh.2012.24010.
- Trevor Park and George Casella. The bayesian lasso. *Journal of the American Statistical Association*, 103(482):681–686, 2008. doi: 10.1198/016214508000000337. URL <https://doi.org/10.1198/016214508000000337>.
- Hong Thom Pham and Bo-Suk Yang. Estimation and forecasting of machine health condition using arma/garch model. *Mechanical systems and signal processing*, 24(2):546–558, 2010.
- Nicholas G. Polson, James G. Scott, and Jesse Windle. Bayesian inference for logistic models using poly-gamma latent variables, 2013.

- Ser-Huang Poon and Stephen J. Taylor. Stock returns and volatility: An empirical study of the uk stock market. *Journal of Banking & Finance*, 16(1):37–59, 1992. ISSN 0378-4266. doi: [https://doi.org/10.1016/0378-4266\(92\)90077-D](https://doi.org/10.1016/0378-4266(92)90077-D). URL <https://www.sciencedirect.com/science/article/pii/037842669290077D>. Special Issue on European Capital Markets.
- R Core Team. *R: A Language and Environment for Statistical Computing*. R Foundation for Statistical Computing, Vienna, Austria, 2013. URL <http://www.R-project.org/>.
- Håvard Rue. Fast Sampling of Gaussian Markov Random Fields. *Journal of the Royal Statistical Society Series B: Statistical Methodology*, 63(2):325–338, 01 2002. ISSN 1369-7412. doi: 10.1111/1467-9868.00288. URL <https://doi.org/10.1111/1467-9868.00288>.
- Esther Ruiz. Quasi-maximum likelihood estimation of stochastic volatility models. *Journal of Econometrics*, 63(1):289–306, 1994. ISSN 0304-4076. doi: [https://doi.org/10.1016/0304-4076\(93\)01569-8](https://doi.org/10.1016/0304-4076(93)01569-8). URL <https://www.sciencedirect.com/science/article/pii/0304407693015698>.
- Rasoul Sajjad, Jerry Coakley, and John C Nankervis. Markov-switching garch modelling of value-at-risk. *Studies in Nonlinear Dynamics & Econometrics*, 12(3), 2008.
- RR Sarkar and C Chatterjee. Application of different time series models on epidemiological data-comparison and predictions for malaria prevalence. *SM J. Biom. Biostat*, 2(4):1022, 2017.
- Toryn L. J. Schafer and David S. Matteson. Locally adaptive shrinkage priors for trends and breaks in count time series. *Technometrics*, 0(ja):1–16, 2024. doi: 10.1080/00401706.2024.2407316. URL <https://doi.org/10.1080/00401706.2024.2407316>.
- Mike K. P. So, K. Lam, and W. K. Li. A stochastic volatility model with markov switching. *Journal of Business & Economic Statistics*, 16(2):244–253, 1998. ISSN 07350015. URL <http://www.jstor.org/stable/1392580>.
- Mike K.P. So, K. Lam, and W.K. Li. An Empirical Study of Volatility in Seven Southeast Asian Stock Markets Using ARV Models. *Journal of Business Finance & Accounting*, 24(2):261–276, March 1997. doi: 10.1111/1468-5957.00104. URL <https://ideas.repec.org/a/bla/jbfnac/v24y1997i2p261-276.html>.
- Fei Su and Lei Wang. Conditional volatility persistence and realized volatility asymmetry: Evidence from the chinese stock markets. *Emerging Markets Finance and Trade*, 56(14):3252–3269, 2020. doi: 10.1080/1540496X.2019.1574566. URL <https://doi.org/10.1080/1540496X.2019.1574566>.
- S.J. Taylor. *Modelling Financial Time Series*. G - Reference, Information and Interdisciplinary Subjects Series. World Scientific, 2008. ISBN 9789812770844. URL <https://books.google.com/books?id=KQ5pDQAAQBAJ>.
- Robert Tibshirani. Regression shrinkage and selection via the lasso. *Journal of the Royal Statistical Society. Series B (Methodological)*, 58(1):267–288, 1996. ISSN 00359246. URL <http://www.jstor.org/stable/2346178>.
- Ryan J. Tibshirani. Adaptive piecewise polynomial estimation via trend filtering. *The Annals of Statistics*, 42(1), February 2014. ISSN 0090-5364. doi: 10.1214/13-aos1189. URL <http://dx.doi.org/10.1214/13-AOS1189>.
- Michael K Tippett. Changing volatility of us annual tornado reports. *Geophysical Research Letters*, 41(19):6956–6961, 2014.

- Huimin Wang, Songbai Song, Gengxi Zhang, Olusola O. Ayantobo, and Tianli Guo. Stochastic volatility modeling of daily streamflow time series. *Water Resources Research*, 59(1):e2021WR031662, 2023a. doi: <https://doi.org/10.1029/2021WR031662>. URL <https://agupubs.onlinelibrary.wiley.com/doi/abs/10.1029/2021WR031662>. e2021WR031662 2021WR031662.
- Huimin Wang, Songbai Song, Gengxi Zhang, and Olusola O. Ayantoboc. Predicting daily streamflow with a novel multi-regime switching arima-ms-garch model. *Journal of Hydrology: Regional Studies*, 47:101374, 2023b. ISSN 2214-5818. doi: <https://doi.org/10.1016/j.ejrh.2023.101374>. URL <https://www.sciencedirect.com/science/article/pii/S2214581823000617>.
- W Wang, PHAJ M Van Gelder, JK Vrijling, and J Ma. Testing and modelling autoregressive conditional heteroskedasticity of streamflow processes. *Nonlinear processes in Geophysics*, 12(1):55–66, 2005.
- MIKE West. On scale mixtures of normal distributions. *Biometrika*, 74(3):646–648, 09 1987. ISSN 0006-3444. doi: [10.1093/biomet/74.3.646](https://doi.org/10.1093/biomet/74.3.646). URL <https://doi.org/10.1093/biomet/74.3.646>.
- Haoxuan Wu, Toryn L. J. Schafer, and David S. Matteson. Trend and variance adaptive bayesian changepoint analysis and local outlier scoring. *Journal of Business & Economic Statistics*, 0(0):1–12, 2024a. doi: [10.1080/07350015.2024.2362269](https://doi.org/10.1080/07350015.2024.2362269). URL <https://doi.org/10.1080/07350015.2024.2362269>.
- Haoxuan Wu, Toryn L. J. Schafer, Sean Ryan, and David S. Matteson. Drift vs shift: Decoupling trends and changepoint analysis. *Technometrics*, 0(ja):1–16, 2024b. doi: [10.1080/00401706.2024.2365730](https://doi.org/10.1080/00401706.2024.2365730). URL <https://doi.org/10.1080/00401706.2024.2365730>.
- Diethelm Wuertz, Yohan Chalabi, Tobias Setz, Martin Maechler, and Georgi N. Boshnakov. *fGarch: Rmetrics - Autoregressive Conditional Heteroskedastic Modelling*, 2023. URL <https://www.rmetrics.org>. R package version 4031.90.